Control of Redundant Flexible Manipulators with Redundancy Resolution

Dipendra Subedi, Ilya Tyapin and Geir Hovland
Department of Engineering Sciences
University of Agder
4879 Grimstad, Norway

Abstract **This paper deals with the online control of a redundant flexible link manipulator to achieve minimum oscillations using the redundancy resolution technique. Different redundancy resolution techniques proposed and used for rigid link manipulators are tested for their use in the case of flexible link manipulators. The simulation model of a planar three-link flexible manipulator is used in this study. The redundancy resolution using kinetic energy minimization techniques is compared with the local joint acceleration minimization method to show the advantage of achieving minimum vibrations.**

E.1 Introduction

In most robotic applications the tasks are specified in the Cartesian space. However, the robot commands are executed in the joint space. Therefore, it is necessary to solve the inverse kinematics problem to find the corresponding joint positions for achieving the desired end-effector position and orientation. A redundant manipulator has more degrees of freedom (DoFs) than required to achieve the desired end-effector position and orientation. The redundant DoFs can be exploited to achieve different criteria for improving the performance of the redundant manipulator without affecting the primary goal of reaching task space configurations (i.e., end-effector position and orientation). Different redundancy resolution methods are available in the literature for rigid link manipulators. Manipulator redundancy has been exploited in the literature to achieve different criteria like joint limits avoidance [1, 2], minimization of kinetic energy [3], obstacles avoidance [4], singularity avoidance [5, 6], and minimization of joint torques [7]. However, their application in redundant flexible link manipulators (FLMs) has not been explored. This work's aim is to explore different redundancy resolution methods and utilize them to control redundant FLMs for achieving minimum vibrations.

Different optimal planning methods have been studied in the literature for the rest-to-rest motion of the FLM to achieve minimum end-effector vibration when approaching a desired final position in the desired traveling time [8, 9]. Particle

swarm optimization algorithms and genetic algorithms have been applied to trajectory planning of flexible redundant manipulators to minimize vibration in [10] and [11] respectively. Although these optimization methods are offline, they require a dynamic model of the FLM which is computationally expensive. Therefore, it is time-consuming and impractical to run the optimization procedure whenever there is a change in the initial position, goal position, or traveling time. The configurations of the FLMs affect the end-effector vibration as highlighted in [12] and [13]. However, there has been little reported work on online control of the FLMs exploiting the redundant configuration of the manipulators for reducing vibrations.

The redundancy resolution methods based on minimum kinetic energy are used in this work for the online control of the FLMs for achieving minimum vibration and compared to the minimum norm joint acceleration solution.

The paper is organized into six sections as follows. Section E.2 describes the kinematics of manipulators. The dynamic model of the planar FLM is presented in section E.3. Different redundancy resolution methods are presented in section E.4. The results obtained from three different redundancy resolution methods when applied to control FLMs are presented in section E.5. Conclusions and discussions follow in section E.6.

E.2 Rigid Body Kinematics

The forward kinematics of a manipulator describing the pose of the end-effector as a function of the joint angles is given by (E.1), where $\boldsymbol{x} \in \mathbb{R}^m$ is the vector representing the pose of the end-effector, and $\boldsymbol{q}_r \in \mathbb{R}^n$ is the vector of joint positions.

$$\boldsymbol{x} = f(\boldsymbol{q}_r) \tag{E.1}$$

For the planar three-link manipulator, $n = 3$ represents three joints and $m = 2$ represents the 2D position of the end-effector. Differentiating (E.1) with respect to time, the relation between joint velocity and end-effector velocity is obtained as shown in (E.2), which is called differential kinematics of the manipulator, where $\boldsymbol{J}(\boldsymbol{q}_r) \in \mathbb{R}^{m \times n}$ is the $m \times n$ Jacobian matrix.

$$\dot{\boldsymbol{x}} = \boldsymbol{J}(\boldsymbol{q}_r)\dot{\boldsymbol{q}}_r \tag{E.2}$$

Similarly, the relation between the joint acceleration and end-effector acceleration is obtained by differentiating (E.2) with respect to time as shown in (E.3).

$$\ddot{\boldsymbol{x}} = \boldsymbol{J}(\boldsymbol{q}_r)\ddot{\boldsymbol{q}}_r + \dot{\boldsymbol{J}}(\boldsymbol{q}_r, \dot{\boldsymbol{q}}_r)\dot{\boldsymbol{q}}_r \tag{E.3}$$

Hereafter, $\boldsymbol{J}$ and $\dot{\boldsymbol{J}}$ are used instead of $\boldsymbol{J}(\boldsymbol{q}_r)$ and $\dot{\boldsymbol{J}}(\boldsymbol{q}_r, \dot{\boldsymbol{q}}_r)$ respectively.

E.3 Manipulator Dynamics

The dynamic model of the planar multi-link flexible manipulator derived using the assumed modes method is given by (E.4), where $\boldsymbol{q} = \begin{bmatrix} \boldsymbol{q}_r & \boldsymbol{q}_f \end{bmatrix}^T$, $\boldsymbol{q}_r = \begin{bmatrix} q_{r1} & q_{r2} & \cdots & q_{rn} \end{bmatrix}^T$, $\boldsymbol{q}_f = \begin{bmatrix} q_{f11} & q_{f12} & \cdots & q_{f1n_f} \cdots & q_{fn1} & q_{fn2} & \cdots & q_{fnn_f} \end{bmatrix}^T$, q_{ri} represents the i^{th} joint position, q_{fij} represents the time-varying variable related to the spatial assumed mode shape of link i and mode of vibration j, n_f represents the total number of assumed modes of vibration, $\boldsymbol{M}(\boldsymbol{q})$ is the inertia matrix, $\boldsymbol{c}(\boldsymbol{q}, \dot{\boldsymbol{q}})$ is the vector of Coriolis and centripetal effects, $\boldsymbol{g}(\boldsymbol{q})$ is the gravity term, and $\boldsymbol{K}$ is the rigidity modal matrix [13].

$$\boldsymbol{M}(\boldsymbol{q})\ddot{\boldsymbol{q}} + \boldsymbol{c}(\boldsymbol{q}, \dot{\boldsymbol{q}}) + \boldsymbol{g}(\boldsymbol{q}) + \boldsymbol{K}\boldsymbol{q} = \boldsymbol{\tau} \tag{E.4}$$

Joint viscous friction and link structural damping can be included by adding a damping matrix $\boldsymbol{D}$ as

$$\boldsymbol{M}(\boldsymbol{q})\ddot{\boldsymbol{q}} + \boldsymbol{c}(\boldsymbol{q}, \dot{\boldsymbol{q}}) + \boldsymbol{g}(\boldsymbol{q}) + \boldsymbol{K}\boldsymbol{q} + \boldsymbol{D}\dot{\boldsymbol{q}} = \boldsymbol{\tau}. \tag{E.5}$$

The dynamic equation can be written in another form separating rigid and flexible parts as in (E.6)–(E.8).

$$\begin{bmatrix} \boldsymbol{M}_{rr} & \boldsymbol{M}_{rf} \\ \boldsymbol{M}_{rf}^T & \boldsymbol{M}_{ff} \end{bmatrix} \begin{bmatrix} \ddot{\boldsymbol{q}}_r \\ \ddot{\boldsymbol{q}}_f \end{bmatrix} + \begin{bmatrix} \boldsymbol{c}_r \\ \boldsymbol{c}_f \end{bmatrix} + \begin{bmatrix} \boldsymbol{g}_r \\ \boldsymbol{g}_f \end{bmatrix} + \begin{bmatrix} \boldsymbol{0} & \boldsymbol{0} \\ \boldsymbol{0} & \boldsymbol{K}_{ff} \end{bmatrix} \begin{bmatrix} \boldsymbol{q}_r \\ \boldsymbol{q}_f \end{bmatrix} + \begin{bmatrix} \boldsymbol{D}_{rr} & \boldsymbol{0} \\ \boldsymbol{0} & \boldsymbol{D}_{ff} \end{bmatrix} \begin{bmatrix} \dot{\boldsymbol{q}}_r \\ \dot{\boldsymbol{q}}_f \end{bmatrix} = \begin{bmatrix} \boldsymbol{\tau}_r \\ \boldsymbol{0} \end{bmatrix} \tag{E.6}$$

$$\boldsymbol{M}_{rr}\ddot{\boldsymbol{q}}_r + \boldsymbol{M}_{rf}\ddot{\boldsymbol{q}}_f + \boldsymbol{c}_r + \boldsymbol{g}_r + \boldsymbol{D}_{rr}\dot{\boldsymbol{q}}_r = \boldsymbol{\tau}_r \tag{E.7}$$

$$\boldsymbol{M}_{rf}^T\ddot{\boldsymbol{q}}_r + \boldsymbol{M}_{ff}\ddot{\boldsymbol{q}}_f + \boldsymbol{c}_f + \boldsymbol{g}_f + \boldsymbol{K}_{ff}\boldsymbol{q}_f + \boldsymbol{D}_{ff}\dot{\boldsymbol{q}}_f = \boldsymbol{0} \tag{E.8}$$

E.4 Redundancy Resolution

A redundant manipulator has more DoFs than required to achieve the desired end-effector position and orientation. That is, the number of DoFs n of a redundant manipulator is greater than the number of controlled end-effector DoFs m. There is an infinite number of robot configurations possible to achieve any given pose of the end-effector.

For redundant manipulators i.e., $n > m$, the general solutions for (E.2) and (E.3)

are given by (E.9) and (E.10) respectively, where $\boldsymbol{J}^+$ represents the pseudoinverse of $\boldsymbol{J}$, $(\boldsymbol{I} - \boldsymbol{J}^+\boldsymbol{J})$ is a projector of arbitrary vectors $\boldsymbol{z}_1 \in \mathbb{R}^n$ and $\boldsymbol{z}_2 \in \mathbb{R}^n$ onto the null space of $\boldsymbol{J}$.

$$\dot{\boldsymbol{q}}_r = \boldsymbol{J}^+\dot{\boldsymbol{x}} + (\boldsymbol{I} - \boldsymbol{J}^+\boldsymbol{J})\boldsymbol{z}_1 \tag{E.9}$$

$$\ddot{\boldsymbol{q}}_r = \boldsymbol{J}^+(\ddot{\boldsymbol{x}} - \dot{\boldsymbol{J}}\dot{\boldsymbol{q}}_r) + (\boldsymbol{I} - \boldsymbol{J}^+\boldsymbol{J})\boldsymbol{z}_2 \tag{E.10}$$

By considering $\boldsymbol{z}_1 = \boldsymbol{0}$ and $\boldsymbol{z}_2 = \boldsymbol{0}$ in (E.9) and (E.10), the pseudoinverse solutions (exact solution) at the velocity and acceleration levels are obtained, which result in the minimum norm joint velocity and minimum norm joint acceleration solutions respectively.

The joint velocity and acceleration solutions given by (E.9) and (E.10) are the solutions of the constrained linear-quadratic optimization problems given by (E.11) and (E.12) respectively.

$$\begin{aligned} \underset{\dot{\boldsymbol{q}}_r}{\text{minimize}} \quad & \boldsymbol{H}(\dot{\boldsymbol{q}}_r) = \frac{1}{2}(\dot{\boldsymbol{q}}_r - \boldsymbol{z}_1)^T(\dot{\boldsymbol{q}}_r - \boldsymbol{z}_1) \\ \text{subject to} \quad & \boldsymbol{J}\dot{\boldsymbol{q}}_r - \dot{\boldsymbol{x}} = \boldsymbol{0} \end{aligned} \tag{E.11}$$

$$\begin{aligned} \underset{\ddot{\boldsymbol{q}}_r}{\text{minimize}} \quad & \boldsymbol{H}(\ddot{\boldsymbol{q}}_r) = \frac{1}{2}(\ddot{\boldsymbol{q}}_r - \boldsymbol{z}_2)^T(\ddot{\boldsymbol{q}}_r - \boldsymbol{z}_2) \\ \text{subject to} \quad & \boldsymbol{J}\ddot{\boldsymbol{q}}_r + \dot{\boldsymbol{J}}\dot{\boldsymbol{q}}_r - \ddot{\boldsymbol{x}} = \boldsymbol{0} \end{aligned} \tag{E.12}$$

The tasks defined by $\boldsymbol{z}_1$ and $\boldsymbol{z}_2$ have no effect on the end-effector motion. Therefore, by choosing suitable vectors $\boldsymbol{z}_1$ and $\boldsymbol{z}_2$, the redundant DoFs could be exploited to optimize certain performance measures (secondary task) without altering the task space configurations (primary goal). Other methods to achieve desired performance characteristics include task augmentation [14] and weighted pseudoinverse technique [3, 7, 15–18].

The general redundancy resolution at velocity and acceleration levels for finding the local optimal motions can be formulated as the constrained linear-quadratic optimization problems given by (E.13) and (E.14) respectively, where $\boldsymbol{W} \in \mathbb{R}^{n\times n}$ is an arbitrary positive-definite symmetric weight matrix.

$$\begin{aligned} \underset{\dot{\boldsymbol{q}}_r}{\text{minimize}} \quad & \boldsymbol{H}(\dot{\boldsymbol{q}}_r) = \frac{1}{2}(\dot{\boldsymbol{q}}_r - \boldsymbol{z}_1)^T\boldsymbol{W}(\dot{\boldsymbol{q}}_r - \boldsymbol{z}_1) \\ \text{subject to} \quad & \boldsymbol{J}\dot{\boldsymbol{q}}_r - \dot{\boldsymbol{x}} = \boldsymbol{0} \end{aligned} \tag{E.13}$$

$$\begin{aligned} \underset{\ddot{\boldsymbol{q}}_r}{\text{minimize}} \quad & \boldsymbol{H}(\ddot{\boldsymbol{q}}_r) = \frac{1}{2}(\ddot{\boldsymbol{q}}_r - \boldsymbol{z}_2)^T\boldsymbol{W}(\ddot{\boldsymbol{q}}_r - \boldsymbol{z}_2) \\ \text{subject to} \quad & \boldsymbol{J}\ddot{\boldsymbol{q}}_r + \dot{\boldsymbol{J}}\dot{\boldsymbol{q}}_r - \ddot{\boldsymbol{x}} = \boldsymbol{0} \end{aligned} \tag{E.14}$$

The solutions of (E.13) and (E.14), which can be derived using Lagrange multipliers, are given by (E.15) and (E.16) respectively, where $\boldsymbol{J}_W^+$ is the weighted pseudoinverse of $\boldsymbol{J}$ given by (E.17).

$$\dot{\boldsymbol{q}}_r = \boldsymbol{J}_W^+ \dot{\boldsymbol{x}} + (\boldsymbol{I} - \boldsymbol{J}_W^+ \boldsymbol{J})\boldsymbol{z}_1 \tag{E.15}$$

$$\ddot{\boldsymbol{q}}_r = \boldsymbol{J}_W^+ (\ddot{\boldsymbol{x}} - \dot{\boldsymbol{J}}\dot{\boldsymbol{q}}_r) + (\boldsymbol{I} - \boldsymbol{J}_W^+ \boldsymbol{J})\boldsymbol{z}_2 \tag{E.16}$$

$$\boldsymbol{J}_W^+ = \boldsymbol{W}^{-1}\boldsymbol{J}^T(\boldsymbol{J}\boldsymbol{W}^{-1}\boldsymbol{J}^T)^{-1} \tag{E.17}$$

In (E.17), the $\boldsymbol{J}_W^+$ becomes ill-conditioned when $\boldsymbol{J}$ is not full (row) rank or when the manipulator reaches a singularity. The singularity problem can be solved by using the Damped-Least-Squares approach which can be formulated as an unconstrained minimization problem of the forms given by (E.18) (at velocity level) and (E.19) (at acceleration level), where a scalar damping or singularity robustness factor λ is used to specify the relative importance of the norms of joint rates/accelerations and the tracking accuracy.

$$\begin{aligned} \underset{\dot{\boldsymbol{q}}_r}{\text{minimize}} \quad \boldsymbol{H}(\dot{\boldsymbol{q}}_r) = \frac{\lambda^2}{2}(\dot{\boldsymbol{q}}_r - \boldsymbol{z}_1)^T \boldsymbol{W}(\dot{\boldsymbol{q}}_r - \boldsymbol{z}_1) \\ + (\boldsymbol{J}\dot{\boldsymbol{q}}_r - \dot{\boldsymbol{x}})^T(\boldsymbol{J}\dot{\boldsymbol{q}}_r - \dot{\boldsymbol{x}}) \end{aligned} \tag{E.18}$$

$$\begin{aligned} \underset{\ddot{\boldsymbol{q}}_r}{\text{minimize}} \quad \boldsymbol{H}(\ddot{\boldsymbol{q}}_r) = \frac{\lambda^2}{2}(\ddot{\boldsymbol{q}}_r - \boldsymbol{z}_2)^T \boldsymbol{W}(\ddot{\boldsymbol{q}}_r - \boldsymbol{z}_2) \\ + (\boldsymbol{J}\ddot{\boldsymbol{q}}_r + \dot{\boldsymbol{J}}\dot{\boldsymbol{q}}_r - \ddot{\boldsymbol{x}})^T(\boldsymbol{J}\ddot{\boldsymbol{q}}_r + \dot{\boldsymbol{J}}\dot{\boldsymbol{q}}_r - \ddot{\boldsymbol{x}}) \end{aligned} \tag{E.19}$$

The solutions of (E.18) and (E.19), which can be derived using Lagrange multipliers, are given by (E.20) and (E.21) respectively, where $\boldsymbol{J}_{W,DLS}^+$ is the damped weighted pseudoinverse of $\boldsymbol{J}$ given by (E.22).

$$\dot{\boldsymbol{q}}_r = \boldsymbol{J}_{W,DLS}^+ \dot{\boldsymbol{x}} + (\boldsymbol{I} - \boldsymbol{J}_{W,DLS}^+ \boldsymbol{J})\boldsymbol{z}_1 \tag{E.20}$$

$$\ddot{\boldsymbol{q}}_r = \boldsymbol{J}_{W,DLS}^+ (\ddot{\boldsymbol{x}} - \dot{\boldsymbol{J}}\dot{\boldsymbol{q}}_r) + (\boldsymbol{I} - \boldsymbol{J}_{W,DLS}^+ \boldsymbol{J})\boldsymbol{z}_2 \tag{E.21}$$

$$\boldsymbol{J}_{W,DLS}^+ = \boldsymbol{W}^{-1}\boldsymbol{J}^T(\boldsymbol{J}\boldsymbol{W}^{-1}\boldsymbol{J}^T + \lambda^2\boldsymbol{I})^{-1} \tag{E.22}$$

It can only be presumed that the sum of squares of joint velocities minimized by the generalized pseudoinverse ((using (E.9)) approximately minimizes the kinetic energy. The inertia-weighted pseudoinverse can be used to realize the true minimization of

kinetic energy [3, 7, 19]. The kinetic energy T of the system is given by (E.23).

$$T = \frac{1}{2}\dot{\boldsymbol{q}}_r^T \boldsymbol{M}_{rr}\dot{\boldsymbol{q}}_r \tag{E.23}$$

The joint acceleration solution of the constrained linear-quadratic optimization problem given by (E.24) that minimizes the manipulator's instantaneous kinetic energy is given by (E.25), where the inertia-weighted pseudoinverse $\boldsymbol{J}_M^+$ used to realize local minimization of kinetic energy is given by (E.26). The inertia-weighted pseudoinverse $\boldsymbol{J}_M^+$ in (E.26) is same as the weighted pseudoinverse in (E.17) with the weighting matrix $\boldsymbol{W} = \boldsymbol{M}_{rr}$.

$$\begin{aligned} \underset{\ddot{\boldsymbol{q}}_r}{\text{minimize}} \quad & \boldsymbol{H}(\ddot{\boldsymbol{q}}_r) = \frac{1}{2}\dot{\boldsymbol{q}}_r^T \boldsymbol{M}_{rr}\dot{\boldsymbol{q}}_r \\ \text{subject to} \quad & \boldsymbol{J}\ddot{\boldsymbol{q}}_r + \dot{\boldsymbol{J}}\dot{\boldsymbol{q}}_r - \ddot{\boldsymbol{x}} = \boldsymbol{0} \end{aligned} \tag{E.24}$$

$$\ddot{\boldsymbol{q}}_r = \boldsymbol{J}_M^+(\ddot{\boldsymbol{x}} - \dot{\boldsymbol{J}}\dot{\boldsymbol{q}}_r) \tag{E.25}$$

$$\boldsymbol{J}_M^+ = \boldsymbol{M}_{rr}^{-1}\boldsymbol{J}^T(\boldsymbol{J}\boldsymbol{M}_{rr}^{-1}\boldsymbol{J}^T)^{-1} \tag{E.26}$$

Similarly, the sum of squares of joint accelerations minimized by the generalized pseudoinverse (using (E.10)) is presumed to approximately minimize the joint torques. Since the manipulators are actually controlled by specifying joint torques to achieve the desired accelerations, it is desirable to optimize joint torques rather than joint velocities or accelerations. Torque minimization methods for redundancy resolution have been thoroughly studied in the literature [3, 6, 7, 16, 18, 20].

In [3], it is shown that the local optimization of the inertia inverse weighted dynamic torque given by (E.27) corresponds to the global kinetic energy minimization problem.

$$\begin{aligned} \underset{\ddot{\boldsymbol{q}}_r}{\text{minimize}} \quad & \boldsymbol{H}(\ddot{\boldsymbol{q}}_r) = \frac{1}{2}\boldsymbol{\tau}_r^T \boldsymbol{M}_{rr}^{-1}\boldsymbol{\tau}_r \\ \text{subject to} \quad & \boldsymbol{J}\ddot{\boldsymbol{q}}_r + \dot{\boldsymbol{J}}\dot{\boldsymbol{q}}_r - \ddot{\boldsymbol{x}} = \boldsymbol{0} \end{aligned} \tag{E.27}$$

The joint acceleration solution of the constrained linear-quadratic minimization problem given by (E.27) derived using Lagrange multipliers is given by (E.28).

$$\ddot{\boldsymbol{q}}_r = \boldsymbol{J}_M^+(\ddot{\boldsymbol{x}} - \dot{\boldsymbol{J}}\dot{\boldsymbol{q}}_r) - (\boldsymbol{I} - \boldsymbol{J}_M^+\boldsymbol{J})\boldsymbol{M}_{rr}^{-1}\boldsymbol{c}_r \tag{E.28}$$

In (E.28), the gravity-related terms are neglected in order to only consider the dynamic effects and to prevent the manipulator configuration from drooping as it attempts to reduce the gravitational potential energy of the system [3, 18]. Moreover, (E.28) is equivalent to (E.16) with the weighting matrix $\boldsymbol{W} = \boldsymbol{M}_{rr}$ and

$\boldsymbol{z}_2 = -\boldsymbol{M}_{rr}^{-1}\boldsymbol{c}_r$.

The joint acceleration solutions using (E.28) leave the joint velocities in the null-space untouched causing the joints that do not contribute to the end-effector motion to move freely. This can make the system unstable. The null space damping method can be used to ensure stability by appending a damping term to the redundant task as given by (E.29), where β is a positive scalar [18, 20].

$$\ddot{\boldsymbol{q}}_r = \boldsymbol{J}_M^{+}(\ddot{\boldsymbol{x}} - \dot{\boldsymbol{J}}\dot{\boldsymbol{q}}_r) - (\boldsymbol{I} - \boldsymbol{J}_M^{+}\boldsymbol{J})(\boldsymbol{M}_{rr}^{-1}\boldsymbol{c}_r + \beta\dot{\boldsymbol{q}}_r) \tag{E.29}$$

The open-loop solutions of joint variables obtained by numerical integration lead to solutions drift and then to task space errors. The Closed-Loop Inverse Kinematics (CLIK) algorithm can be used to overcome the joint drift problem which is based on the task space error between the desired and the actual end-effector positions or the task space velocity error [1]. The CLIK algorithm with redundancy resolution at the acceleration level is shown in Fig. E.1, where $\boldsymbol{K}_p$ and $\boldsymbol{K}_v$ are symmetric positive definite matrices and their choices guarantee that the task-space position error ($\boldsymbol{e}_p = \boldsymbol{x}_d - \boldsymbol{x}$) and velocity error ($\boldsymbol{e}_v = \dot{\boldsymbol{x}}_d - \boldsymbol{J}\dot{\boldsymbol{q}}_r$) uniformly converge to zero. The joint trajectories generated using the redundancy resolution techniques are used for the online control of the FLM as shown in Fig. E.1.

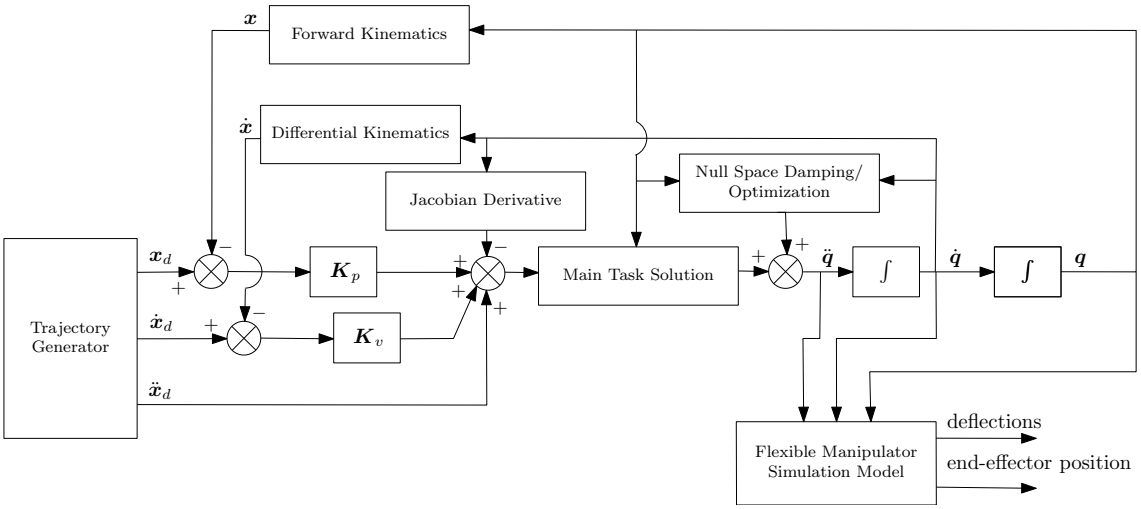

Figure E.1: CLIK algorithm with redundancy resolution at the acceleration level.

E.5 Simulation Results

A planar three-link flexible manipulator with three revolute joints ($n = 3$) is used in the simulation for the end-effector position control in the 2D Cartesian space ($m = 2$). Each link of the flexible arm is made of a hollow aluminium profile of length $\ell_1 = \ell_2 = \ell_3 = 1.5$ m. Each joint consists of a hub, motor, and planetary gearbox.

The simulation parameters of the FLM are detailed in [13].

Fig. E.2 shows the equivalent rigid body schematic of a three-link manipulator with Denavit-Hartenberg (DH) parameters given in Table E.1.

The quintic trajectory generator is used to generate a smooth Cartesian trajectory to move the end-effector from the initial position ($x_0 = \begin{bmatrix} 3 & 1.5 \end{bmatrix}^T$) to goal position ($x_f = \begin{bmatrix} 2 & 2 \end{bmatrix}^T$) in 0.5 s. The end-effector position, velocity, and acceleration trajectories used in this paper are shown in Fig. E.3. Since the flexible dynamics of the FLM is simulated for 2 s (to study about the residual oscillations) the trajectories are shown for the whole simulation time. The method proposed in [12] is used to estimate the optimal initial configuration of the redundant arm representing weak-vibration configuration.

The flexible dynamics of the FLM is simulated for 2 s using (E.8), where the joint trajectories are generated using different redundancy resolution techniques (see Fig. E.1). *MATLAB ode45* is used for time integration of dynamic equation given by (E.8). The joint trajectories generated using the redundancy resolution techniques are fed to the simulation model of the FLM to study the effects in the flexible dynamics of the FLM as shown in Fig. E.1. Following three cases of redundancy resolution methods are compared for their use in FLMs:

1. Case A: Local minimization of the joint acceleration (LMJA).

$$\begin{aligned} \ddot{\boldsymbol{q}}_r = \boldsymbol{J}^+((\ddot{\boldsymbol{x}}_d + \boldsymbol{K}_p(\boldsymbol{x}_d - \boldsymbol{x}) + \boldsymbol{K}_v(\dot{\boldsymbol{x}}_d - \boldsymbol{J}\dot{\boldsymbol{q}})) \\ - \dot{\boldsymbol{J}}\dot{\boldsymbol{q}}_r) + (\boldsymbol{I} - \boldsymbol{J}^+\boldsymbol{J})(-\beta\dot{\boldsymbol{q}}_r) \end{aligned} \tag{E.30}$$

   Here, $\boldsymbol{K}_p$ and $\boldsymbol{K}_v$ are symmetric positive definite matrices and their choices guarantee that the task-space position and velocity errors uniformly converge to zero.

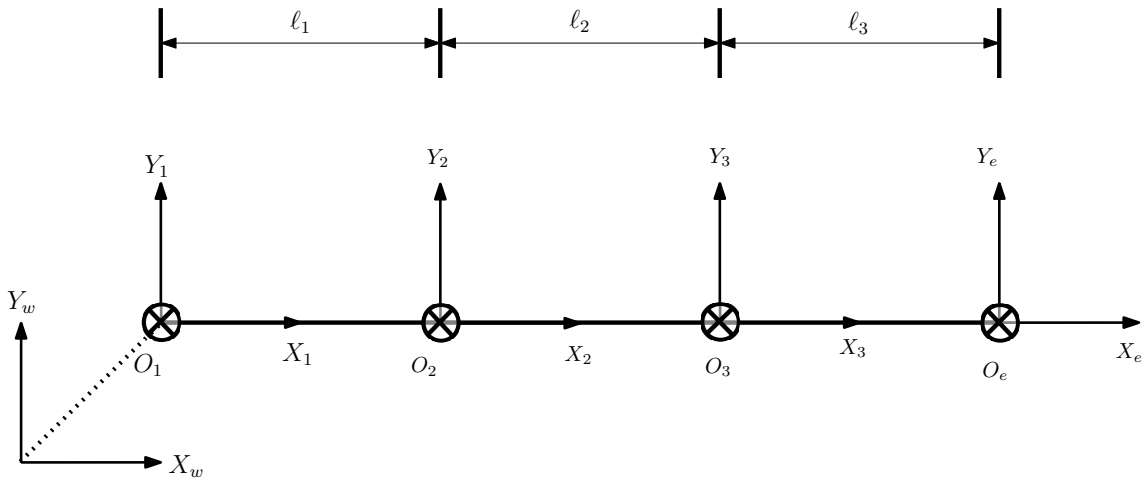

Figure E.2: Equivalent rigid body kinematics.

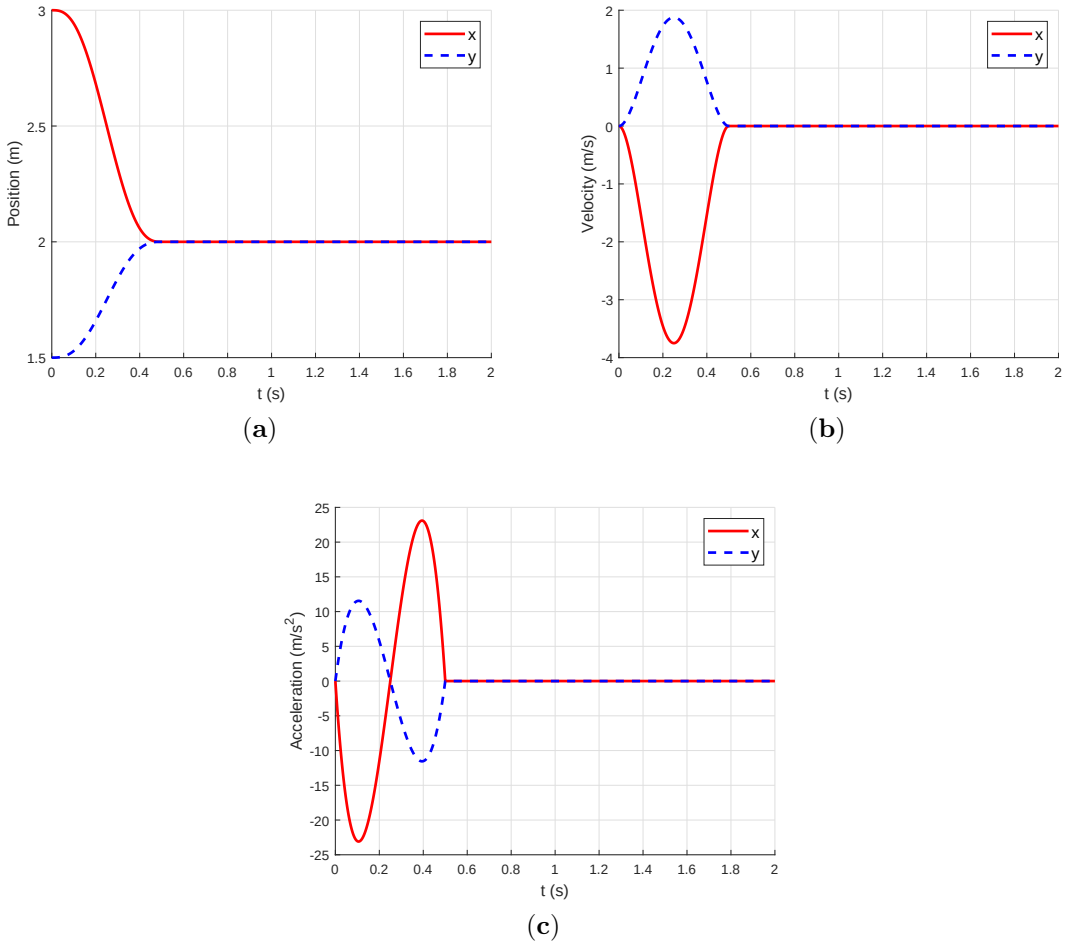

Figure E.3: End-effector trajectories (**a**) position, (**b**) velocity, and (**c**) acceleration.

2. Case B: Local minimization of the kinetic energy (LMKE).

$$\begin{aligned}\ddot{\boldsymbol{q}}_r = \boldsymbol{J}_M^{+}((\ddot{\boldsymbol{x}}_d + \boldsymbol{K}_p(\boldsymbol{x}_d - \boldsymbol{x}) + \boldsymbol{K}_v(\dot{\boldsymbol{x}}_d - \boldsymbol{J}\dot{\boldsymbol{q}}) \\ - \dot{\boldsymbol{J}}\dot{\boldsymbol{q}}_r) + (\boldsymbol{I} - \boldsymbol{J}^{+}\boldsymbol{J})(-\beta\dot{\boldsymbol{q}}_r)\end{aligned} \tag{E.31}$$

3. Case C: Local minimization of the inertia inverse weighted dynamic driving force or global minimization of the kinetic energy (GMKE).

$$\begin{aligned}\ddot{\boldsymbol{q}}_r = \boldsymbol{J}_M^{+}((\ddot{\boldsymbol{x}}_d + \boldsymbol{K}_p(\boldsymbol{x}_d - \boldsymbol{x}) + \boldsymbol{K}_v(\dot{\boldsymbol{x}}_d - \boldsymbol{J}\dot{\boldsymbol{q}}) \\ - \dot{\boldsymbol{J}}\dot{\boldsymbol{q}}_r) - (\boldsymbol{I} - \boldsymbol{J}_M^{+}\boldsymbol{J})(\boldsymbol{M}_{rr}^{-1}\boldsymbol{c}_r + \beta\dot{\boldsymbol{q}}_r)\end{aligned} \tag{E.32}$$

Table E.1: DH PARAMETERS

Axis	**TranZ**	**RotZ**	**TranX**	**RotX**
1	0.0	q_{r1}	ℓ_1	0.0
2	0.0	q_{r2}	ℓ_2	0.0
3	0.0	q_{r3}	ℓ_3	0.0

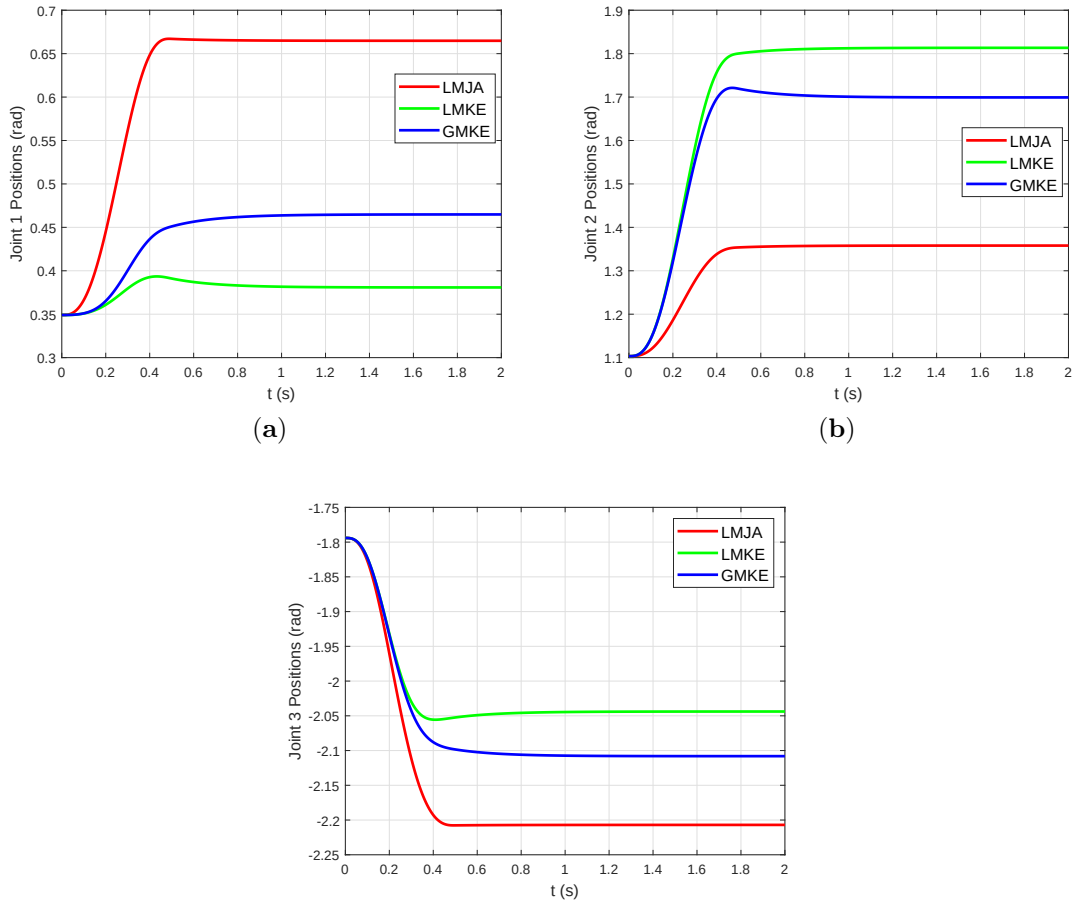

Figure E.4: Joint trajectories when using different redundancy resolution methods (**a**) joint 1 position, (**b**) joint 2 position, and (**c**) joint 3 position.

All the above cases have been implemented with $\beta = 5$, $\boldsymbol{K}_p = \begin{bmatrix} 1 & 0 \\ 0 & 1 \end{bmatrix}$, and $\boldsymbol{K}_v = \begin{bmatrix} 1 & 0 \\ 0 & 1 \end{bmatrix}$. The forward Euler method is used with a step size of 1×10^{-4} s to integrate the joint accelerations to obtain joint velocities and positions. The joint position trajectories obtained by integrating joint acceleration solutions given by (E.30)–(E.32) are shown in Fig. E.4. Although the manipulator starts with the same initial configuration in all three cases, the final joint configurations are different. The final joint configuration has an effect on the residual vibration of the end-effector [12, 13].

The link deflections and end-effector position, shown in Fig. E.5, are estimated using the assumed modes method as presented in [13]. The simulation model of the FLM (given by (E.7) and (E.8)) is used only to show the flexible dynamics of the FLM when applying different redundancy resolution techniques. The online control method with redundancy resolution used in this paper is not based on the dynamic

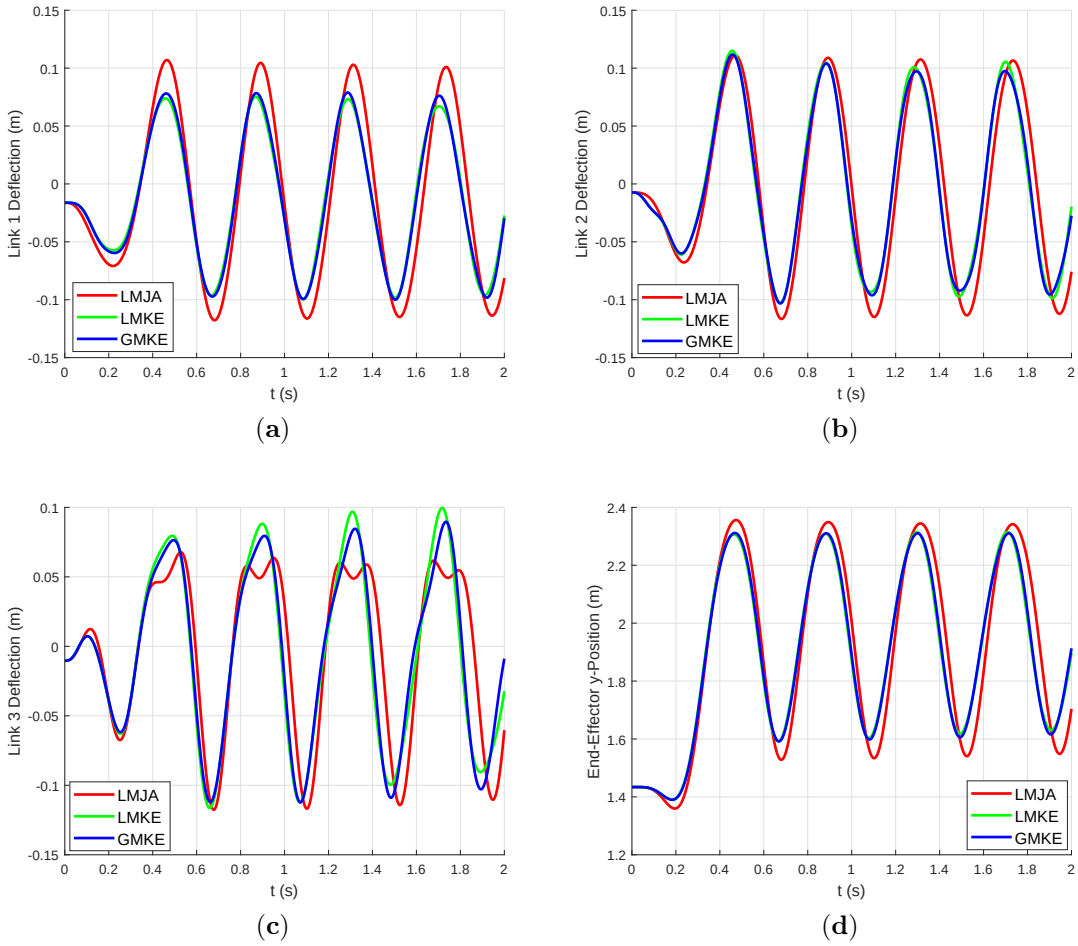

Figure E.5: Link deflections and end-effector y-position when using different redundancy resolution methods (**a**) Link 1 deflection, (**b**) Link 2 deflection, (**c**) Link 3 deflection, and (**d**) End-effector y-position.

model of the FLM. However, the inertia matrix ($\boldsymbol{M}_{rr}$) and the vector of Coriolis and centripetal effects ($\boldsymbol{c}_r$) equivalent to the rigid model of the FLM are used in case of kinetic energy minimization approaches of redundancy resolution.

Fig. E.5 shows that the link-tip deflections with respect to its base and the end-effector vibration when using the kinetic energy minimization methods of redundancy resolution are lower compared to the minimum joint acceleration method. Moreover, there is not much difference visible (see Fig. E.5) in the vibration minimization when using the global kinetic energy minimization method compared to the local kinetic energy minimization method.

E.6 Conclusion

Different methods to control redundant manipulators using redundancy resolution techniques are presented. The redundancy resolution by minimizing kinetic energy

is compared to the solution obtained from local minimization of joint acceleration concerning elastic vibration in the FLM. The results proved that the kinetic energy minimization approaches reduce the elastic vibrations compared to the local joint acceleration minimization method. Although, the kinetic energy minimization approaches of redundancy resolution use the inertia matrix ($\boldsymbol{M}_{rr}$) and the vector of Coriolis and centripetal effects ($\boldsymbol{c}_r$) equivalent to the rigid model of the FLM, these methods can still be used for the online control of the FLM. This is because only the rigid parts of the inertia matrix $\boldsymbol{M}$ and the vector of Coriolis and centripetal effects $\boldsymbol{c}$ are used in the online control of the FLM.

In the next step, it is worth testing the redundancy resolution methods, aimed at reducing elastic vibrations, in the actual experimental setup of the FLM.

Acknowledgment

The work was partially funded by the Research Council of Norway through the centre SFI Offshore Mechatronics, project 237896.

References – Paper E

[1] Jingguo Wang, Yangmin Li, and Xinhua Zhao. Inverse kinematics and control of a 7-DOF redundant manipulator based on the closed-loop Algorithm. *International Journal of Advanced Robotic Systems*, 7(4):1–9, 2010. ISSN 17298814. doi: 10.5772/10495.

[2] Fabrizio Flacco, Alessandro De Luca, and Oussama Khatib. Control of Redundant Robots under Hard Joint Constraints: Saturation in the Null Space. *IEEE Transactions on Robotics*, 31(3):637–654, 2015. ISSN 15523098. doi: 10.1109/TRO.2015.2418582.

[3] A. Nedungadi and K. Kazerouinian. A Local Solution with Global Characteristics for the Joint Torque Optimization of a Redundant Manipulator. *Advanced Robotics: 1989*, 6(5):559–591, 1989. doi: 10.1007/978-3-642-83957-3_39.

[4] M Kirćanski and M Vukobratović. *Trajectory Planning for Redundant Manipulators in the Presence of Obstacles*, pages 57–63. Springer US, Boston, MA, 1985. ISBN 978-1-4615-9882-4. doi: 10.1007/978-1-4615-9882-4_6.

[5] Charles W Wampler. Manipulator Inverse Kinematic Solutions Based on Vector Formulations and Damped Least-Squares Methods. *IEEE Transactions on Systems, Man, and Cybernetics*, 16(1):93–101, 1986. doi: 10.1109/TSMC.1986.289285.

[6] C. Y. Chung, B. H. Lee, M. S. Kim, and C. W. Lee. Torque optimizing control with singularity-robustness for kinematically redundant robots. *Journal of Intelligent and Robotic Systems: Theory and Applications*, 28(3):231–258, 2000. ISSN 09210296. doi: 10.1023/A:1008152705719.

[7] John M. Hollerbach and Ki C. Suh. Redundancy resolution of manipulators through torque optimization. In *Proceedings - IEEE International Conference on Robotics and Automation*, pages 1016–1021, 1985. ISBN 0818606150. doi: 10.1109/ROBOT.1985.1087285.

[8] M Benosman, G Le Vey, L Lanari, and A De Luca. Rest-to-Rest Motion for Planar Multi-Link Flexible Manipulator Through Backward Recursion. *Journal*

of Dynamic Systems, Measurement, and Control, 126(1):115–123, apr 2004. ISSN 0022-0434. doi: 10.1115/1.1649976.

[9] M. H. Korayem, A. Nikoobin, and V. Azimirad. Trajectory optimization of flexible link manipulators in point-to-point motion. *Robotica*, 27(6):825–840, 2009. ISSN 02635747. doi: 10.1017/S0263574708005183.

[10] Pengfei Xin, Jili Rong, Yongtai Yang, Dalin Xiang, and Yang Xiang. Trajectory planning with residual vibration suppression for space manipulator based on particle swarm optimization algorithm. *Advances in Mechanical Engineering*, 9 (4):1–16, 2017. ISSN 16878140. doi: 10.1177/1687814017692694.

[11] Shigang Yue, Dominik Henrich, W. L. Xu, and S. K. Tso. Point-to-point trajectory planning of flexible redundant robot manipulators using genetic algorithms. *Robotica*, 20(3):269–280, 2002. ISSN 02635747. doi: 10.1017/S0263574701003861.

[12] Yue Shigang. Weak-vibration configurations for flexible robot manipulators with kinematic redundancy. *Mechanism and Machine Theory*, 35(2):165–178, 2000. ISSN 0094114X. doi: 10.1016/S0094-114X(98)00071-8.

[13] Dipendra Subedi, Ilya Tyapin, and Geir Hovland. Dynamic Modeling of Planar Multi-Link Flexible Manipulators. *Robotics*, 10(2), 2021. ISSN 2218-6581. doi: 10.3390/robotics10020070.

[14] Pyung Chang. A closed-form solution for inverse kinematics of robot manipulators with redundancy. *IEEE Journal on Robotics and Automation*, 3(5):393–403, 1987. doi: 10.1109/JRA.1987.1087114.

[15] Daniel E. Whitney. Resolved Motion Rate Control of Manipulators and Human Prostheses. *IEEE Transactions on Man-Machine Systems*, 10(2):47–53, 1969. ISSN 21682860. doi: 10.1109/TMMS.1969.299896.

[16] B. Hu, C. L. Teo, and H. P. Lee. Local Optimization of Weighted Joint Torques for Redundant Robotic Manipulators. *IEEE Transactions on Robotics and Automation*, 11(3):422–425, 1995. ISSN 1042296X. doi: 10.1109/70.388785.

[17] Yunong Zhang, Shuzhi Sam Ge, and Tong Heng Lee. A unified quadratic-programming-based dynamical system approach to joint torque optimization of physically constrained redundant manipulators. *IEEE Transactions on Systems, Man, and Cybernetics, Part B: Cybernetics*, 34(5):2126–2132, 2004. ISSN 10834419. doi: 10.1109/TSMCB.2004.830347.

[18] Jon Woolfrey, Wenjie Lu, and Dikai Liu. A Control Method for Joint Torque Minimization of Redundant Manipulators Handling Large External Forces.

Journal of Intelligent and Robotic Systems: Theory and Applications, 96(1): 3–16, 2019. ISSN 15730409. doi: 10.1007/s10846-018-0964-8.

[19] O Khatib. A unified approach for motion and force control of robot manipulators: The operational space formulation. *IEEE Journal on Robotics and Automation*, 3(1):43–53, 1987. doi: 10.1109/JRA.1987.1087068.

[20] H.-J. Kang and R A Freeman. Joint torque optimization of redundant manipulators via the null space damping method. In *Proceedings 1992 IEEE International Conference on Robotics and Automation*, pages 520–525 vol.1, 1992. doi: 10.1109/ROBOT.1992.220239.